# Direct observation of intermediates in the SufS cysteine desulfurase reaction reveals functional roles of conserved active-site residues

Received for publication, May 21, 2019, and in revised form, June 16, 2019 Published, Papers in Press, June 27, 2019, DOI 10.1074/jbc.RA119.009471

**Matthew Blahut[‡], Courtney E. Wise[‡], Michael R. Bruno[§], Guangchao Dong[‡], Thomas M. Makris[‡], Patrick A. Frantom[§], Jack A. Dunkle[§1], and F. Wayne Outten[‡2]**

*From the [‡]Department of Chemistry and Biochemistry, University of South Carolina, Columbia, South Carolina 29208 and the [§]Department of Chemistry and Biochemistry, University of Alabama, Tuscaloosa, Alabama 35487*

Edited by F. Peter Guengerich

**Iron-sulfur (Fe-S) clusters are necessary for the proper functioning of numerous metalloproteins. Fe-S cluster (Isc) and sulfur utilization factor (Suf) pathways are the key biosynthetic routes responsible for generating these Fe-S cluster prosthetic groups in *Escherichia coli*. Although Isc dominates under normal conditions, Suf takes over during periods of iron depletion and oxidative stress. Sulfur acquisition via these systems relies on the ability to remove sulfur from free cysteine using a cysteine desulfurase mechanism. In the Suf pathway, the dimeric SufS protein uses the cofactor pyridoxal 5′-phosphate (PLP) to abstract sulfur from free cysteine, resulting in the production of alanine and persulfide. Despite much progress, the stepwise mechanism by which this PLP-dependent enzyme operates remains unclear. Here, using rapid-mixing kinetics in conjunction with X-ray crystallography, we analyzed the pre-steady-state kinetics of this process while assigning early intermediates of the mechanism. We employed H123A and C364A SufS variants to trap Cys-aldimine and Cys-ketimine intermediates of the cysteine desulfurase reaction, enabling direct observations of these intermediates and associated conformational changes of the SufS active site. Of note, we propose that Cys-364 is essential for positioning the Cys-aldimine for Cα deprotonation, His-123 acts to protonate the Ala-enamine intermediate, and Arg-56 facilitates catalysis by hydrogen bonding with the sulfhydryl of Cys-aldimine. Our results, along with previous SufS structural findings, suggest a detailed model of the SufS-catalyzed reaction from Cys binding to C–S bond cleavage and indicate that Arg-56, His-123, and Cys-364 are critical SufS residues in this C–S bond cleavage pathway.**

This work was supported by National Institutes of Health NIGMS Grant GM112919 (to F. W. O. and P. A. F.) and in part by a grant from the University of South Carolina Office of Research (to T. M. M. and F. W. O.). The authors declare that they have no conflicts of interest with the contents of this article. The content is solely the responsibility of the authors and does not necessarily represent the official views of the National Institutes of Health.

This article contains Figs. S1–S7 and Tables S1–S2.

*The atomic coordinates and structure factors (codes 6O10, 6O11, 6O12, and 6O13) have been deposited in the Protein Data Bank (http://wwpdb.org/).*

[1] To whom correspondence may be addressed. Tel.: 205-348-0269; Fax: 205-348-9104; E-mail: jadunkle@ua.edu.

[2] To whom correspondence may be addressed. Tel.: 803-777-8151; Fax: 803-777-9521; E-mail: woutten@sc.edu.

Iron-sulfur (Fe-S) clusters perform vital functions in a myriad of reactions including electron transfer, amino acid biosynthesis, and central carbon metabolism (1, 2). Despite their significance, a number of questions still remain regarding the mechanism through which Fe-S clusters are generated. To avoid the inherent toxicity of sulfide and labile iron, most organisms use a carefully orchestrated *in vivo* Fe-S cluster biogenesis pathway controlled by protein–protein interactions. Production of these important clusters in *Escherichia coli* occurs via two major pathways, Isc and Suf (3). Although Isc directs Fe-S generation under normal conditions, Suf dominates in environments of oxidative stress and iron starvation (4–7).

Encoded by the *suf* operon, the Suf system in *E. coli* consists of six proteins responsible for the biogenesis and transfer of Fe-S clusters to the apo form of target Fe-S metalloproteins. The pyridoxal 5′-phosphate (PLP)[3]-dependent homodimeric SufS enzyme provides the sulfide component of the Fe-S cluster (8). SufS belongs to a family of cysteine desulfurases responsible for liberating sulfur from free cysteine resulting in an enzyme-bound *S*-sulfanylcysteine species (often referred to as a persulfide). The desulfurase activity is usually coupled via a ping-pong mechanism to a second transpersulfuration step where the persulfide species is transferred from the active-site cysteine residue to acceptor proteins or metabolites (9, 10).

The cysteine desulfurase enzymes are divided into two separate groups depending on their structures and reactivity (11). Type I desulfurases have high basal activity and an extended and flexible active-site loop. Type II desulfurase family members conversely have diminished basal activity along with a shortened active-site anchor that limits structural flexibility and solvent access to the persulfide intermediate after the desulfurase reaction (12, 13). Type II enzymes often interact with a partner protein that enhances their activity by specifically accepting the persulfide from the enzyme in a transpersulfuration reaction that completes the entire ping-pong reaction (14). For example, the *E. coli* type II enzyme SufS requires acceptor protein SufE to remove the persulfide from SufS active-site Cys-364 to allow turnover (15, 16). Transpersulfuration from

[3] The abbreviations used are: PLP, pyridoxal 5′-phosphate; βME, β-mercaptoethanol; PDA, photodiode array; PMT, photomultiplier tube; SVD, singular value decomposition; XDS, X-ray detector software; SHMT, serine hydroxymethyltransferase; PDB, Protein Data Bank; HDX-MS, hydrogen-deuterium exchange-MS.

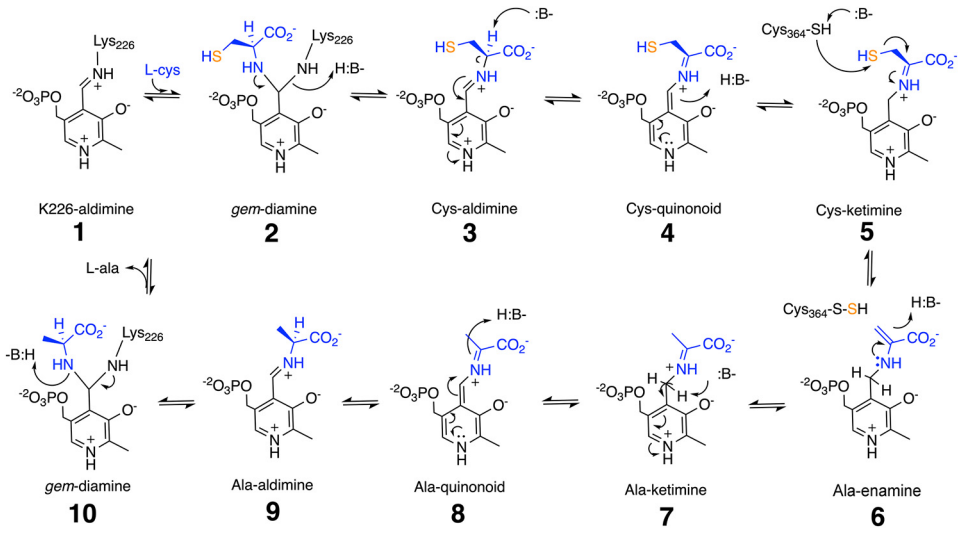


**SCHEME 1. General cysteine desulfurase reaction scheme for SufS prior to this study.** L-Cysteine substrate is shown in *blue* (C, H, O, and N) and *orange* (S). PLP and SufS active-site residues are in *black*.

SufS Cys-364 to SufE Cys-51 is carried out via a thiol exchange mechanism when the two proteins interact. SufE, carrying the *S*-sulfanylcysteine species, will then transfer the persulfide to the $SufBC_2D$ scaffold complex to be reduced to sulfide and incorporated into nascent Fe-S cluster (17).

A proposed chemical mechanism for SufS, based on other characterized cysteine desulfurase enzymes, is shown in Scheme 1 (18–20). Resting SufS contains PLP bound to Lys-226 in an internal aldimine (Schiff base) conformation (**1**) (10). As shown in Scheme 1, upon L-cysteine substrate binding, a *gem*-diamine intermediate is formed (**2**) followed by formation of the Cys-aldimine (**3**) (sometimes referred to as the external aldimine). The Cys-aldimine converts to a short-lived Cys-quinonoid intermediate (**4**) followed by a Cys-ketimine (**5**). The desulfurase step occurs as Cys-364 carries out a nucleophilic attack on the substrate sulfur, converting the Cys-ketimine into the Ala-enamine and forming a persulfide on Cys-364 (**6**). Mutation of active-site Cys-364 to alanine results in the elimination of cysteine desulfurase activity (21). The alanine product is ultimately released and the internal aldimine regenerated between PLP and Lys-226 (**6**–**10**). As the detailed mechanism demonstrates, there are several important acid-base catalysis steps involved in the desulfurase reaction, including the deprotonation of $C_\alpha$ on the cysteine substrate, deprotonation of Cys-364 to generate the nucleophilic thiolate anion, protonation of the Cys-quinonoid C4′ to facilitate formation of the Cys-ketimine, and protonation of the Ala-enamine following C–S bond breakage (Scheme 1).

The exact active-site residues that carry out these acid-base catalyst steps are presently unknown. Multiple sequence alignments indicate His-123 is a highly conserved residue in the active site that could potentially be involved in proton transfer during SufS cysteine desulfurase activity (Fig. 1*A*). Wild-type (WT) SufS crystal structures indicate His-123 forms a $\pi$–$\pi$ stacking interaction with the PLP aromatic group and is optimally located to function as an acid-base catalyst during the desulfurase reaction (Fig. 1*B*) (22). Based on the these observations, it was previously proposed to play such a role (18).

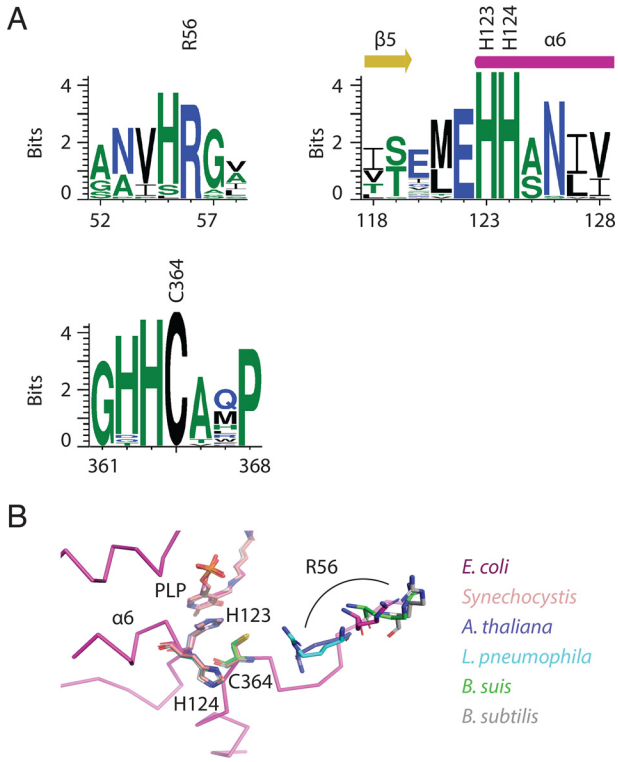


**Figure 1.** *A,* a sequence logo indicates active-site residues of interest that are highly conserved across SufS proteins. The sequence alignment was made from 29 members of the InterPro SufS family (IPR010970) chosen from distinct nodes of a sequence similarity network to model sequence diversity in the family. *B,* a structural superposition of six SufS family members from the PDB reveals that several residues, such as His-123 and His-124, adopt an identical position in all structures, while the location of Arg-56 (indicated by an *arc*) varies.

Recent structural characterization by Dunkle *et al.* (23) focused on conformational changes thought to be associated with transpersulfuration. The new structures reported here investigate the mechanism of the desulfurase reaction. Here, we have mutated His-123 and Cys-364 to alanine and performed a detailed analysis of WT, C364A, and H123A SufS enzymes using UV-visible absorption spectroscopy, transient kinetics via stopped-flow spectroscopy, and X-ray crystallography. The

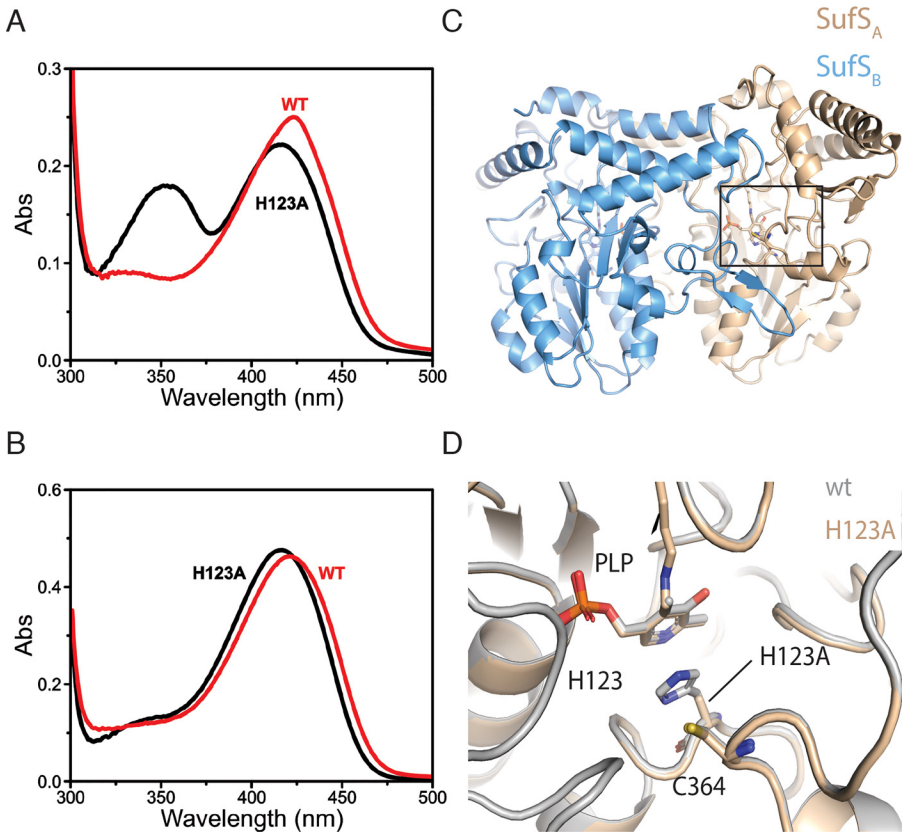


**Figure 2.** *A,* UV-visible absorption spectra for fractions containing WT or H123A SufS from the initial purification step using an anion exchange column. *B,* UV-visible absorption spectra for fractions containing WT or H123A SufS from the second purification step using a hydrophobic interaction column. Presence of SufS was confirmed in all fractions by SDS-PAGE. *C,* an image of the SufS homodimer including a *box* denoting the active-site region shown below. *D,* a superposition of WT SufS and SufS H123A reveals that the mutation does not affect the position of other critical active-site components such as PLP or Cys-364.

**Table 1**

**Cysteine desulfurase activity for SufS and its mutant derivatives**

Desulfurase assays were performed in triplicate. Error shown (±) indicates one S.D. above and below the average.

| SufS | Persulfide generated per SufS | Persulfide generated per SufS + SufE[a] |
|---|---|---|
| | $\mu$M/$\mu$M | |
| WT | 1.10 ± 0.06 | 16.1 ± 1.2 |
| H123A | 0.09 ± 0.01 | 0 |
| C364A | 0.07 ± 0.02 | 0 |

[a] 1 $\mu$M SufS with 4 $\mu$M SufE.

two active-site mutants assisted in trapping Cys-aldimine and Cys-ketimine intermediates of the cysteine desulfurase reaction. As a result, the mutants facilitated the direct structural observation of these two reaction intermediates and associated conformational changes to the SufS active site. Emerging from the analysis is a rich picture of the functional roles of several amino acids conserved across the SufS family including the unanticipated, essential role of Cys-364 in positioning the Cys-aldimine for $C_\alpha$ deprotonation, and the essential role of His-123 in protonating the Ala-enamine intermediate.

## Results

### *A metastable substrate-PLP intermediate in the reaction of SufS H123A with cysteine*

During and after purification of WT and C364A SufS, a PLP absorption feature at ~422 nm is observed (Fig. 2*A* and data not shown). The 422 nm feature is assigned as the Lys-226–PLP internal aldimine. In contrast, after the first anion exchange step of purification, the SufS H123A fractions showed a more complex spectrum consisting of two absorption maxima at 418 and 350 nm (Fig. 2*A*). As the purification proceeds through additional chromatographic steps, the 350-nm absorption feature in SufS H123A is gradually lost (Fig. 2*B*). This feature at 350 nm will be further elaborated on below. The final PLP absorbance after purification of SufS H123A shows a slight decrease in extinction coefficient along with a subtle blue shift to around 418 nm, compared with 422 nm observed in WT SufS. WT and the mutant forms of SufS were all confirmed to have greater than 95% PLP occupancy following purification (see "Experimental procedures" for details).

To test if the H123A mutation alters the ability of the mutant SufS to complete the first half of the ping-pong reaction, persulfide production by WT, C364A, and H123A enzymes was measured (Table 1). Due to the lack of the active-site thiolate anion, the C364A mutant of SufS should not be able to form persulfide. The results in Table 1 show that both the H123A and C364A mutations abolish the ability of SufS to generate persulfide from L-cysteine. The addition of the SufE partner protein had no effect on the activity of either mutant SufS protein (Table 1). In contrast, WT SufS, in the absence of SufE, carries out a single turnover reaction producing 1 eq of persulfide. Under these conditions, using DTT as the reductant, SufS stops upon completion of the first half of the ping-pong reaction because the persulfide species is resistant to reduction by DTT.

When SufE is added to WT SufS, it removes the SufS persulfide as part of the transpersulfuration reaction. The SufE persulfide is accessible to DTT and is reduced to sulfide under these conditions, allowing SufE to perform additional cycles of transpersulfuration (10). These results suggest the substrate-PLP intermediate trapped in the SufS H123A mutant has not yet been desulfurated.

The crystal structure was solved for SufS H123A and the resulting $F_o - F_c$ difference electron density maps indicated the presence of PLP in agreement with the chemical analysis. A superposition of the mutant homodimer with the WT SufS homodimer revealed that the two structures were near identical with an root mean square deviation of 0.159 Å (Fig. 2, *C* and *D*). This result suggests that the unusual spectral characteristics of PLP within SufS H123A observed during purification were due to the loss of the $\pi-\pi$ stacking or H-bonding interactions from His-123 rather than long-range structural changes in or around the active site.

It was previously shown that upon binding to L-cysteine, the PLP absorption spectrum in WT SufS shows a decrease in the 422-nm signal and the appearance of a feature at 340 nm (13). To better define the altered optical features noted during purification of the SufS H123A variant, UV-visible absorption spectra were taken before and after the addition of varying concentrations of the L-cysteine substrate (Fig. 3 and Fig. S1). Immediately after the addition of 500 $\mu$M cysteine to WT SufS, decrease of the internal aldimine peak at 422 nm was observed along with a subtle red shift of that feature to 424 nm (Fig. S1*A*). These changes coincided with a concomitant increase of the feature at 343 nm (Fig. 3*A*). Following the completion of the desulfurase reaction after the consumption of cysteine (~150 min after 500 $\mu$M cysteine is added), the internal aldimine at 422 nm is restored (Fig. 3*A*).

The optical changes observed in steady-state reactions of the SufS mutants were distinctly altered from WT SufS. As noted above, prior to L-cysteine addition, the spectrum of purified H123A SufS is characterized by a single major absorption feature at 418 nm. Upon the addition of excess cysteine, H123A shows a greater accumulation of a species at the same 350 nm feature that is observed during purification (Figs. 2*A* and 3*B*). In contrast to WT or C364A SufS, relatively little signal is observed in the 420-nm region. Based on the observation that the addition of L-cysteine can reproduce the 350-nm species, we tentatively assign this feature to a substrate-PLP intermediate that is captured by the H123A mutation. This 350-nm species is stable as it is still present 150 min after L-cysteine addition (Fig. 3*B*), which is in agreement with the results presented in Fig. 2. Kinetic monitoring of the peak at 350 nm over time did not show any reversibility of this feature over 150 min (data not shown).

Upon the addition of excess L-cysteine to C364A SufS, the resting state 422-nm peak is partially converted to a species with absorbance at 343 and 424 nm similar to the spectrum obtained for WT SufS (Fig. S1*B* and Fig. 3*C*). However, unlike WT SufS, C364A did not revert back to the resting state at 422 nm, even to 150 min. These results suggest that the H123A and C364A mutations can trap different PLP-substrate intermediates.

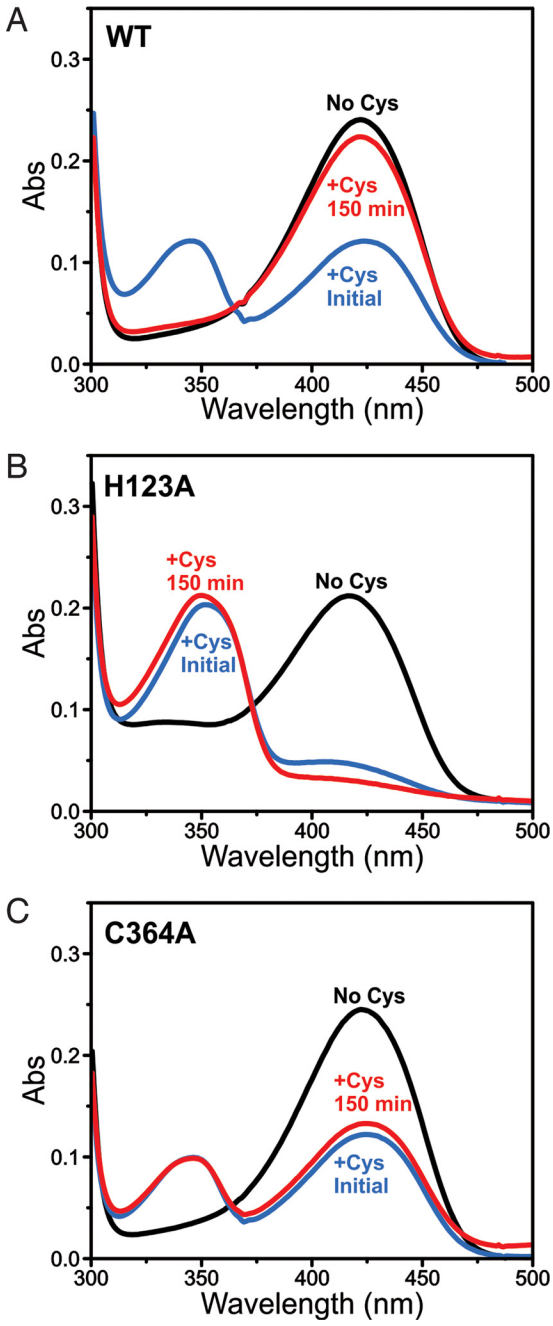


**Figure 3. UV-visible absorption spectra during 150 min treatment with 500 $\mu$M L-cysteine for (*A*) WT, (*B*) H123A, and (*C*) C364A SufS.**

### *Pre-steady-state stopped-flow kinetic analysis of WT and mutant SufS reaction intermediates*

Standard cysteine desulfurase assays measure the persulfide or alanine products of the first half of the ping-pong reaction and neither approach can be used to analyze individual reaction steps prior to L-cysteine desulfuration. Therefore, stopped-flow UV-visible absorption spectroscopy in both photodiode array (PDA) and photomultiplier tube (PMT) modes was used to analyze the progression of reaction intermediates upon mixing of L-cysteine with SufS and its mutants. WT, H123A, or C364A SufS was rapidly mixed with varying concentrations of anoxic L-cysteine at 4 °C. Initial examination of the WT SufS reaction via stopped-flow absorption spectroscopy using the PDA

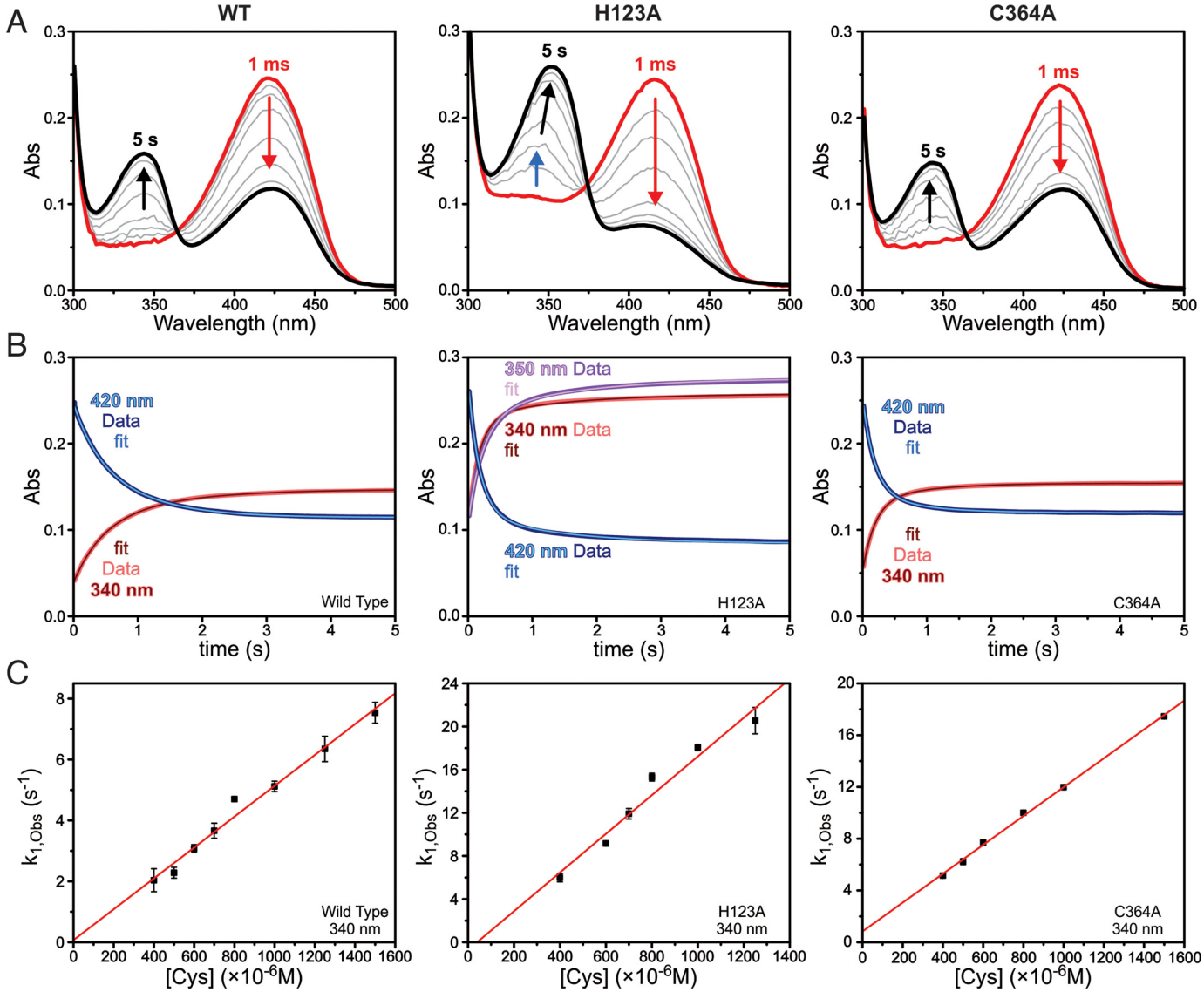


**Figure 4. Stopped-flow analysis of 37.5 $\mu$M (post-mix) WT (*left*), H123A (*center*), and C364A SufS (*right*) with various cysteine concentrations.** *A,* absorbance spectrum at various time points for the reaction of 400 $\mu$M cysteine with SufS. *B,* absorbance *versus* time traces monitored at 340 and 420 nm for 400 $\mu$M cysteine mixed with SufS. *C,* fast phase ($1/\tau_1$) at different cysteine concentrations monitored at 340 nm (in which $1/\tau_1$ is the reciprocal relaxation time).

detector revealed a concerted shift from 422 nm to the 343- and 424-nm species with a clear isosbestic point for the transitions (Fig. 4*A*). Fitting the changes in 343- and 422-nm absorbances over time measured by the PMT detector required a two-summed exponential equation for each wavelength, representing two kinetically distinguishable steps involved in formation of the 343-nm species (see "Experimental procedures") (Fig. 4*B*, Table 2). The two phases are split between an initial, cysteine-dependent fast phase and a cysteine-independent slow phase. A zero-intercept for the former fast phase suggests an essentially irreversible binding of cysteine to the PLP cofactor ($k_1$ = 5.1 $mM^{-1}$ $s^{-1}$) followed by a slower step ($k_2$ = 1.4 $s^{-1}$) (Fig. 4*C*, Table 2).

The general absorption changes of the C364A SufS mutant (transition from 422 to 343 and 424 nm with a clear isosbestic point) are highly similar to those observed in WT SufS (Fig. 4*A* and Fig. S2). The derived kinetic rate constants ($k_1$ = 11 $mM^{-1}$ $s^{-1}$, $k_2$ = 1.6 $s^{-1}$) are also similar to that of the WT enzyme (Table 2). These similarities indicate that the steps being monitored at 340 and 420 nm likely correspond to early stages in the ping-pong mechanism prior to L-cysteine desulfuration.

**Table 2**
**Comparison of SufS stopped-flow data collected in PMT mode at the indicated wavelengths**

| Protein and phase | Wavelength | |
|---|---|---|
| | 340 nm | 350 nm (for H123A only) |
| WT SufS, $k_{fast}$ ($M^{-1}$ $s^{-1}$) | 5.1 (±0.3) × $10^3$ | – |
| H123A SufS, $k_{fast}$ ($M^{-1}$ $s^{-1}$) | 1.8 (±0.2) × $10^4$ | 1.3 (±0.1) × $10^4$ |
| C364A SufS, $k_{fast}$ ($M^{-1}$ $s^{-1}$) | 1.1 (±0.1) × $10^4$ | – |
| WT SufS, $k_{slow}$ ($s^{-1}$) | 1.4 ± 0.3 | – |
| H123A SufS, $k_{slow}$ ($s^{-1}$) | 1.3 ± 0.1 | 1.3 ± 0.1 |
| C364A SufS, $k_{slow}$ ($s^{-1}$) | 1.6 ± 0.1 | – |

In contrast to WT and C364A SufS, the reaction of L-cysteine with the H123A mutant exhibits a more complex kinetic process. The blue-shifted internal aldimine at 418 nm is consumed without a concomitant appearance of the 424-nm species,

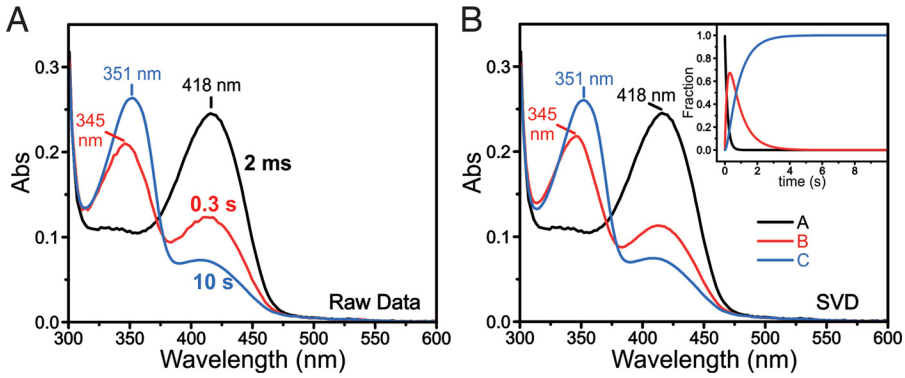


**Figure 5. UV-visible absorption features of 37.5 $\mu$M H123A SufS (post-mix) with 400 $\mu$M L-cysteine fit to an A to B to C transition, where A, B, and C represent distinct species (see text for details).** *A*, spectra obtained from the indicated time points after mixing of H123A SufS and cysteine. *B*, pure component spectra of H123A SufS determined using global fitting SVD analysis of PDA data. *B, inset*, fractional concentration of each species in the H123A SufS spectra over time after L-cysteine addition.

regardless of the L-cysteine concentration. These results closely match the effects noted in steady-state experiments (Figs. 2*A* and 3*B*). The complexity of this process is evidenced by a clear lack of isosbestic points during the transitions (Fig. 4*A* and Fig. S2). An initial intermediate with a $\lambda_{max} \sim 345$ nm is quickly formed within ~300 ms followed by a much slower shift to a species at ~350 nm over the following 4.7 s (Fig. 4*A* and Fig. S3). The latter absorption feature at 350 nm is identical to that observed in the steady-state reactions described above (Fig. 3*B*). Global analysis by singular value decomposition (SVD) was used to analyze the PDA data to further establish that two distinct intermediates are formed in the reaction of H123A SufS with L-cysteine. The evolution of PDA spectra could not be adequately fit with a single kinetic process, but minimally required two steps and the inclusion of a spectroscopically distinguishable intermediate at 345 nm (Fig. 5). Like C364A, the derived kinetic rate constants for H123A ($k_1 = 18\ mM^{-1}\ s^{-1}$, $k_2 = 1.3\ s^{-1}$) are similar to those for the WT enzyme (Table 2).

### *The X-ray crystal structure of a SufS Cys-aldimine*

The intermediates formed upon incubation of SufS mutants with L-cysteine were structurally characterized. First, the diffraction data were measured on a WT SufS crystal incubated with L-cysteine. In agreement with previous experiments, this did not yield electron density for a trapped intermediate but instead showed electron density for a sub-stoichiometric amount of Cys-364-persulfide, the product of the cysteine desulfurase reaction (Fig. S4) (23, 24). Next, the structure of SufS C364A was solved following incubation of the crystal with L-cysteine. The crystallization conditions have a pH of 7 with PEG as the precipitant and therefore possess a native chemical environment for the enzyme. Diffraction data were collected to 1.85 Å and the structure was solved by molecular replacement using PDB 1jf9 with all heteroatoms removed. The resulting unbiased $F_o - F_c$ difference electron density maps revealed a strong signal for a ligand covalently bound to PLP and a lack of electron density between Lys-226 and PLP indicating the loss of the Lys-aldimine (Fig. 6*A*). The electron density indicated the presence of seven non-H atoms in the ligand consistent with a Cys-aldimine intermediate. Inspection of the $C_\alpha$ atom revealed tetrahedral geometry suggesting the substrate $C_\alpha$ was participating in four covalent bonds as expected for the Cys-aldimine intermediate (Fig. 6*A*). We also measured anomalous diffraction data on the Cys-soaked C364A crystal with 1.74-Å X-rays and observed an anomalous signal confirming the presence of the S atom in the ligand and its identity as Cys-aldimine (Fig. 6*B*). Additional anomalous signal is present for the P atom of PLP as expected and also for a solvent ion, most likely $Cl^-$ adjacent to Cys-364 (Fig. 6*B*). In summary the data indicate the C364A mutation blocked progression of cysteine desulfurase chemistry at the Cys-aldimine step.

To determine whether additional changes to the structure of SufS C364A occurred upon formation of the Cys-aldimine state, a superposition of the homodimer with the WT SufS homodimer was performed (Fig. 6*C*). The superposition indicated no gross structural changes resulted upon formation of the Cys-aldimine state but revealed a restructuring of a loop adjacent to the active site (Fig. 6*C*). The loop contains the Arg-56 residue that forms a hydrogen bond to the sulfhydryl of the Cys-aldimine intermediate, an interaction that may play a role in substrate $C_\alpha$ deprotonation (Fig. 6*C*).

### *The X-ray crystal structure of a SufS Cys-ketimine*

To determine the identity of the reaction intermediate observed by UV-visible absorption spectroscopy, the structure of SufS H123A incubated with L-cysteine was solved. SufS H123A crystals at pH 6.5 with NaCl as the precipitant were incubated with L-cysteine and then frozen in liquid $N_2$ for X-ray data collection. During incubation with L-cysteine, the crystals gradually lost their yellow color, associated with 420 nm absorbance, and became clear (Fig. 7*A*). Molecular replacement was used to solve the structure. Unbiased $F_o - F_c$ difference electron density maps possessed a strong signal for a reaction intermediate, containing seven non-H atoms covalently linked to PLP (Fig. 7*B*). Inspection of the geometry at the substrate $C_\alpha$ indicated a trigonal planar arrangement of atoms surrounding $C_\alpha$, consistent with a Cys-ketimine, a reaction intermediate formed just prior to C–S bond cleavage (Scheme 1, Fig. 7*B*). Anomalous diffraction data were collected and the corresponding maps indicated the presence of an S atom in the position expected for Cys-ketimine (Fig. 7*C*).

A superposition was performed between the homodimer of SufS H123A in the Cys-ketimine state and the WT SufS homodimer (Fig. 7*D*). The alignment intimated that the two

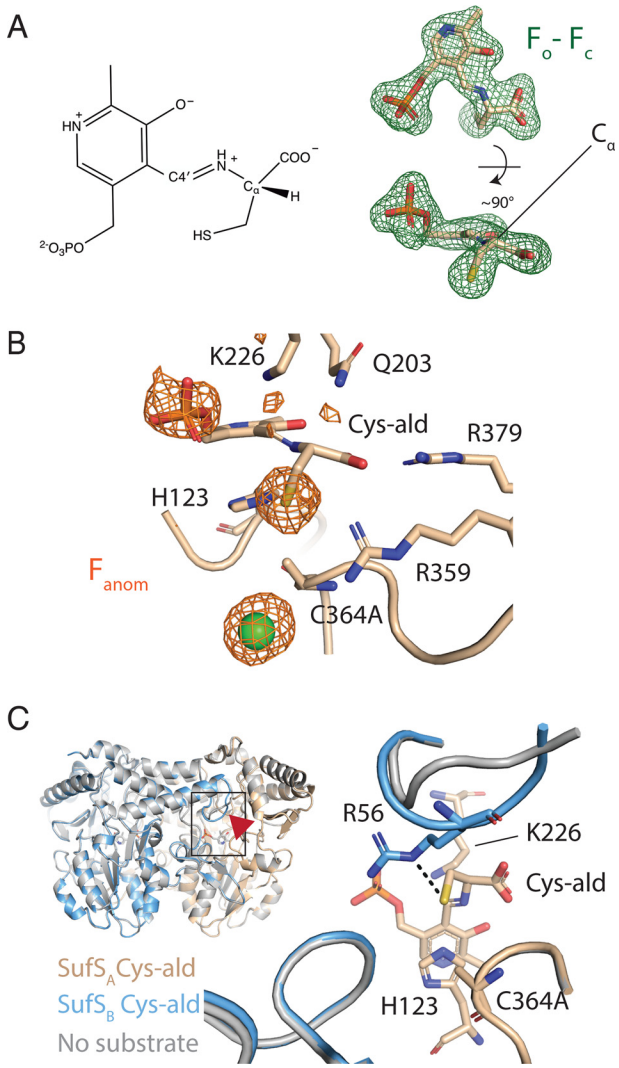


**Figure 6.** *A,* unbiased $F_o - F_c$ difference electron density maps of C364A crystals incubated with L-cysteine possess electron density for a Cys-aldimine enzymatic intermediate covalently bound to PLP. A tetrahedral arrangement of the atoms bonded to $C_\alpha$ indicates $sp^3$ hybridization consistent with assignment of the intermediate as Cys-aldimine. A line drawing of Cys-aldimine is also shown. *B,* anomalous electron density maps of the active-site of SufS C364A with Cys-aldimine, contoured at 3 $\sigma$, possess a strong signal indicating the presence of the Cys-aldimine S atom. Anomalous signals are also observed corresponding to the P atom of PLP and a solvent molecule that is most likely $Cl^-$. *C,* a superposition of SufS Cys-364 with Cys-aldimine in the active-site *versus* SufS WT with no substrate is shown. A *sharp kink* in the region of Arg-56 in SufS monomer B unfurls to allow hydrogen bonding between Arg-56 and the sulfhydryl of Cys-aldimine.

SufS H123A monomers had rotated relative to one another partially altering electrostatic interactions at the dimer interface (Fig. 7*D*). Because SufS H123A and WT SufS are superimposable in the absence of a ligand (see Fig. 2, *C* and *D*), these data suggest that formation of the Cys-ketimine state is coincident with a reordering of the SufS subunits relative to one another. Previous HDX-MS studies of SufS dynamics indicated that dimer rearrangement is associated with reaction progression (25).

## Discussion

Early sequence analysis of cysteine desulfurases identified two distinct groups of enzymes: type I typified by IscS or NifS and type II enzymes exemplified by SufS (11). Recent automated sequence analysis by InterPro confirms these early results clustering ~19,000 sequences together in the IPR010970, SufS family. SufS homologs are present in the genomes of Gram-positive and Gram-negative bacteria, cyanobacteria, and plant plastids. SufS model systems have emerged from each of these phylogenetic groups with SufS deletion mutant phenotypes and SufS interacting partners having been described by several groups (10, 13, 16, 17, 26, 27). Although SufS is not essential in *E. coli* due to functional overlap with IscS, genetic investigations of SufS in *Bacillus subtilis*, *Synechocystis*, and *Arabidopsis thaliana* have found that it is indispensable in each of these organisms. Furthermore, the role of SufS in Fe-S cluster biosynthesis has been confirmed in multiple model organisms (10, 13, 26). The function of conserved active-site residues in the mechanism of SufS, however, is not well-resolved. Using new data reported here, alongside existing SufS structural data, we composed a model detailing the progression of SufS from Cys binding to C–S bond cleavage (Scheme 2 and Fig. 8). Our results highlight new functions of Arg-56, His-123, and Cys-364 in the steps on the pathway to C–S bond cleavage.

### *Assignment of PLP intermediates in UV-visible spectra*

The identification and characterization of PLP intermediates in enzymes is often complicated by significant overlap in their spectral properties and that several species can coexist in rapid equilibria. For example, both internal and external aldimine species are expected to absorb in the 400–420–nm region. However, tautomerization from the ketoenamine to the enolimine form of aldimine results in a shift in absorbance to the 330-nm region as well (28). The 330–350–nm region is also home to absorbance maxima from the *gem*-diamine and ketimine-PLP intermediates (29, 30). Only the quinonoid-PLP intermediate has a distinct absorption spectra with a peak in the 500-nm region (31, 32). Given these complications, integration of the kinetic and structural data described above are essential for assignment.

Results from UV-visible and stopped-flow monitored rapid reaction experiments show that all three enzymes share an initial step upon exposure to L-cysteine, conversion of the stable resting state ~420 nm species (assigned as the internal Lys-226–aldmine) to new species at 340–345 and 424 nm. The linear dependence of the fast phase on cysteine concentration and zero-intercept suggest that this step is dominated by the rate constant of the cysteine binding step. The irreversible nature of this stage, which may be anticipated for formation of a covalent PLP adduct, uncouples the slow phase from cysteine. The rate of this transition is very similar in all three enzymes suggesting the two substitutions have not affected this step in the reaction.

Absorbance in the 340-nm region is consistent with either a ketimine or *gem*-diamine PLP intermediate. Assignment of the initial 343-nm signal as the ketimine intermediate is not supported by the spectroscopic and structural results with H123A SufS described below. Furthermore, the *gem*-diamine intermediate is short-lived with typical formation rates >45 $s^{-1}$ and would therefore be unlikely to accumulate on the time scale of

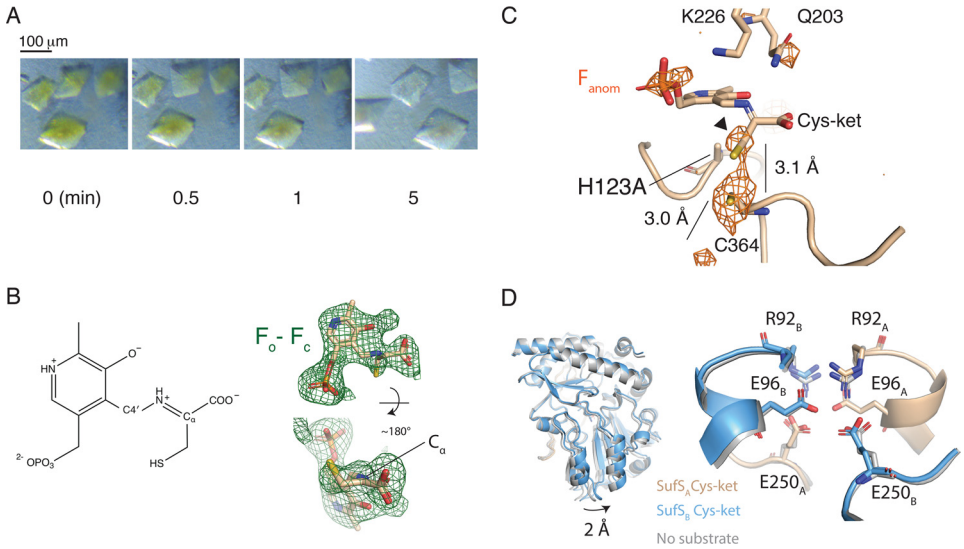


**Figure 7.** *A,* crystals of SufS H123A lose 420 nm absorbance (loss of *yellow color*) upon incubation with L-cysteine. *B,* unbiased $F_o - F_c$ difference electron density maps of H123A crystals incubated with L-cysteine possess electron density for a Cys-ketimine enzymatic intermediate covalently bound to PLP. A planar arrangement of the atoms bonded to $C_\alpha$ indicates $sp^2$ hybridization consistent with assignment of the intermediate as Cys-ketimine. A line drawing of Cys-ketimine is also shown. *C,* anomalous difference electron density maps of the active-site of SufS H123A with Cys-ketimine, contoured at 3 $\sigma$, possess a strong signal indicating the position of the Cys-ketimine S atom. Anomalous signals are also observed corresponding to the S atom of Cys-364 and a solvent atom adjacent to Cys-364. The solvent atom has been previously observed in WT SufS structures and is most likely $Cl^-$. A weak anomalous signal is observed for the P atom of PLP. *D,* a superposition of SufS H123A without substrate and H123A in the Cys-ketimine state reveals rotation of the SufS monomers occurs in the Cys-ketimine state. Subtle changes to the electrostatic interactions at the SufS dimer interface occur as part of the monomer rotation.

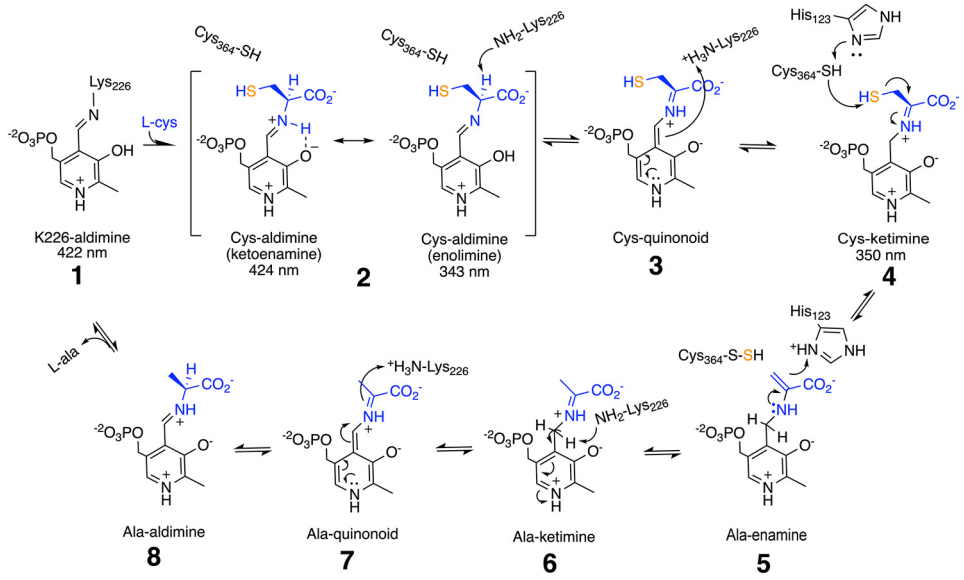


**SCHEME 2. Updated cysteine desulfurase reaction scheme for SufS based on results presented in this work.** L-Cysteine substrate is shown in *blue* (C, H, O, and N) and *orange* (S). PLP and SufS active-site residues are in *black*.

minutes as observed in WT and C364A SufS upon L-cysteine addition (Figs. 2 and 3) (20, 29, 33).

As mentioned above, the external Cys-aldimine can exist in two tautomers with distinct UV-visible absorption maxima in the 340- and 420-nm regions. In some cases, such as for the cyanobacterial C-DES enzyme, these species are stable over a time scale of minutes (34). The structure of C364A SufS clearly shows the external Cys-aldimine as the trapped intermediate, although X-ray crystallography cannot distinguish the individual tautomers (Fig. 6). Because the C364A SufS has an absorption spectra upon L-cysteine binding very similar to WT SufS (Fig. 3), we assign the 343- and 424-nm species formed upon L-cysteine binding in WT and C364A SufS as the enolimine and ketoenamine tautomers of the Cys-aldimine, respectively (Scheme 2, **2**).

The failure to observe further reaction intermediates beyond the Cys-aldimine tautomers in the WT SufS reaction with L-cysteine was unexpected. On sufficiently long time scales of multiple minutes, WT SufS by itself can undergo a single turnover (Table 1) (9, 10). However, the rate of persulfide production by SufS alone is ~0.12 ((nmol of product $min^{-1}$)/(nmol of SufS)). Under the stopped-flow conditions, using ~5.6 nmol of SufS, it would take 8.3 min to produce 1 eq of persulfide. This relative lack of activity over these short time scales is consistent

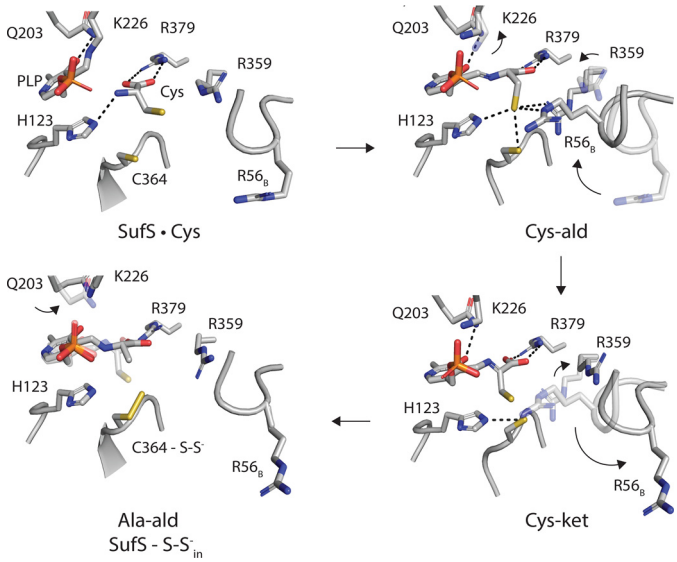


**Figure 8. The roles of active-site residues in the SufS cysteine desulfurase mechanism.** Active-site residues implicated in type II cysteine desulfurase function are labeled. *Arrows* show residues that change conformation during reaction progression. *Dotted lines* represent hydrogen bonds or electrostatic interactions. SufS-S-$S^-_{in}$ indicates the persulfide covalently linked to SufS Cys-364 is positioned toward PLP. Coordinate super-positions used to generate the model are described under "Experimental procedures." SufS bound to L-cysteine is derived from PDB 5db5. The Cys-aldimine and Cys-ketimine structures were created by modeling Cys-364 or His-123 into the corresponding mutant structures (PDB codes 6O11 and 6O13). The Ala-aldimine structure was modeled by combining PDB 1i29 (external aldimine) and PDB 6mr2 (S-$S^-_{in}$ and Arg-56).

with the lack of observable intermediates beyond the Cys-aldimine stage of the cysteine desulfurase reaction for WT SufS.

For true catalytic activity, SufS requires the SufE persulfide acceptor. It is possible that the stalling of the WT reaction at the Cys-aldimine stage when SufS is alone reflects coordinated regulation of the combined cysteine desulfurase-transpersulfuration reaction. Because *E. coli* SufS is specifically expressed under conditions that disrupt Fe-S cluster metabolism, including oxidative stress, the enzyme may remain in the Cys-aldimine state until the SufE acceptor interacts with it. This regulation would prevent premature formation of the reactive persulfide species prior to having SufE present to accept the persulfide from SufS Cys-364. It has previously been shown that the SufS–SufE persulfide generation is more resistant to disruption by $H_2O_2$ than other Type I cysteine desulfurases like IscS (9). Further experiments are underway to test if SufE regulates the cysteine desulfurase activity of SufS (in addition to participating in the transpersulfuration reaction).

In contrast to the relative stability of the 343/424-nm spectra produced in WT and C364A SufS, H123A SufS forms a transient 345-nm peak in the first 0.3 s after mixing with L-cysteine, which rapidly converts to a stable species with a peak absorbance of 350 nm. The stable 350-nm species is assigned as the Cys-ketimine intermediate on the basis of several lines of evidence. Electron density in the crystal structure of H123A SufS can be fit well with the Cys-ketimine structure (Fig. 7*B*). Additionally, both the anomalous diffraction (Fig. 7*C*) and kinetic data (Table 1) are consistent with an intact C–S bond on the PLP intermediate. The initial 345-nm peak formed upon L-cysteine binding to H123A SufS is assigned as the enolimine tautomer of the Cys-aldimine that is slightly red-shifted by loss of the nearby histidine and its $\pi-\pi$ stacking interaction. This assignment is also consistent with known PLP chemistry because the enolimine is predicted to be the more reactive of the Cys-aldimine tautomers and would logically proceed to the Cys-ketimine seen at 350 nm (35, 36).

### *A role for His-123 as an acid-base catalyst*

The finding that loss of His-123 in SufS traps the Cys-ketimine intermediate (Figs. 3 and 8) suggests a key mechanistic role for His-123 in catalysis. Structurally, His-123 is adjacent to the PLP ring where it can influence the PLP cofactor through $\pi-\pi$ stacking interactions. Although tyrosine and phenylalanine residues are often found in this position in aminotransferase enzymes, decarboxylase enzymes commonly utilize a histidine (36). Based on the structural evidence, His-123 is optimally placed to act in an acid/base capacity to deprotonate/protonate the C4′ position of the PLP (2.7 Å) in a step involving Cys-ketimine formation or to interact with the $C_\alpha$ (3.1 Å) or $C_\beta$ (2.7 Å) of the amino acid-PLP adduct. Identification of the Cys-ketimine intermediate in the H123A variant rules out His-123 as the residue responsible for protonation at the C4′ position to form the ketimine (conversion of **4** to **5** in Scheme 1). A role for $C_\alpha$ protonation/deprotonation is also ruled out as the proton is located on the face of the $C_\alpha$ atom pointing away from His-123. This leaves interactions at the $C_\beta$ position as the only viable option. His-123 acting to protonate the PLP-Ala-enamine after C–S bond cleavage (Scheme 1, **6**) fits nicely with the structural and spectroscopic data as a stalled Ala-enamine would likely revert back to the more stable Cys-ketimine. His-123 is also located near the sulfhydryl group of Cys-364 (4.1 Å) and could play a role in deprotonation of the nucleophilic −SH group prior to C–S bond cleavage as well as protonating the resulting Ala-enamine intermediate after C–S bond cleavage.

The ability of the H123A SufS mutant to move beyond the Cys-aldimine to the Cys-ketimine stage of the reaction while both WT and C364A remain at that earlier step is at first puzzling. However, loss of $\pi-\pi$ stacking interactions with PLP in the H123A mutant seems to favor accumulation of the enolimine tautomer of the Cys-aldimine as seen by the asymmetry in 343/424-nm signal intensity (Figs. 3–5). A similar phenomenon is predicted by metadynamics calculations carried out on the PLP-dependent serine hydroxymethyltransferase (SHMT) enzyme (35). Those previous studies suggested that the $\pi-\pi$ interaction of the PLP pyridine ring with SHMT His-122 is weakened in the enolimine tautomer of the external aldimine of SHMT. This shift in the equilibrium between Cys-aldimine tautomers may explain the ability of the H123A SufS to move to the Cys-ketimine intermediate before stalling.

### *A role for Cys-364 in orienting $C_\alpha$ toward catalysis*

The identification of the external Cys-aldimine as the trapped intermediate in C364A seems counterintuitive at first glance. Loss of C364A should prevent C–S bond cleavage, which one would predict to stall at the Cys-ketimine intermediate. Nonetheless, the lack of persulfide production and detailed structural results are consistent with C364A SufS being stalled at the Cys-aldimine intermediate. Therefore, Cys-364

may play a mechanistic role in conversion of the Cys-aldimine to the Cys-ketimine intermediate. Cys-364 is too far from the $C_\alpha$ to act directly in the deprotonation step. The simplest interpretation of these results is that Cys-364 engages in a hydrogen-bonding interaction with the $S_\gamma$ atom of Cys-aldimine required to properly position $C_\alpha$ for deprotonation by another active-site residue.

### *Lys-226 is likely responsible for $C_\alpha$-H bond breakage to form the Cys-ketimine intermediate*

On the basis of the Cys-aldimine structure, it appears the Lys-226, which forms the Schiff base linkage with the internal PLP aldimine, is responsible for the 1,3 proton shift to generate the Cys-ketimine intermediate from the Cys-aldimine. In the structure, the side chain of Lys-226 is positioned 3.4 Å from the C4′ position of PLP and 4.8 Å from the $C_\alpha$ position. There is a wide pocket of space for the residue to sample, and it is the only potential acid/base residue on the correct face for $C_\alpha$ deprotonation. Under the current experimental conditions, lack of an observable intermediate with absorbance around 500 nm in the H123A SufS reaction suggests that either the quinonoid species decomposes faster than it is formed or that the ketimine species is formed directly from the anionic intermediate.

### *A detailed mechanism for SufS*

Taking all of the data together, a detailed mechanism can be proposed for the desulfurase reaction catalyzed by SufS in the absence of SufE (Scheme 2). In the first step, L-cysteine reacts with the internal aldimine (**1**) to form a *gem*-diamine species that rapidly converts to a mix of enolimine (343 nm) and ketoenamine (424 nm) tautomers of the Cys-aldimine (**2**). This concerted process occurs with a second-order rate constant of $\sim$5000 $M^{-1}$ $s^{-1}$. As this equilibrium state is the sole intermediate state, deprotonation of the $C_\alpha$ position is likely rate-determining in the desulfurase reaction with all subsequent steps in the return to Lys-226 –aldimine occurring rapidly. Lys-226 can act as a general base to deprotonate the $C_\alpha$ position forming the Cys-quinonoid intermediate (**3**), which is not observable under current reaction conditions. Lys-226 may then transfer the proton to the C4′ position on PLP converting it to the Cys-ketimine intermediate (350 nm) (**4**). Following formation of the Cys-ketimine, Cys-364 attacks the sulfhydryl on the Cys-ketimine to break the C–S bond. His-123 may assist in this step by deprotonating Cys-364 to produce the nucleophilic sulfide form. The Ala-enamine (**5**) produced by C–S bond cleavage is protonated by His-123 to produce the Ala-ketimine intermediate (**6**). Lys-226 then acts as an acid/base catalyst to cycle back to the Ala-aldimine species (**7** and **8**). Finally, Lys-226 stimulates release of L-alanine and formation of the internal aldmine while passing through a transient *gem*-diamine species. It is important to note that these experiments were performed in the absence of the persulfide acceptor SufE, which limits SufS to no more than a single turnover under these conditions (and in fact less than a full turnover as noted above). Addition of SufE to the system certainly impacts the transpersulfurase activity of SufS by providing the physiological substrate for the second half of the ping-pong reaction. The addition of SufE greatly enhances SufS activity up to 200-fold over SufS alone. Previous studies have suggested that SufE also influences the SufS active-site allosterically and could impact specific steps in the cysteine desulfurase reaction as well (37, 38).

### *SufS conformational changes during reaction progression*

The spectroscopic analysis of WT, H123A, and C364A SufS show that all three proceed with L-cysteine binding through a biphasic process with similar kinetic rate constants. The fast phase of 340 nm formation represents formation of the Cys-aldimine tautomers in all three enzymes. However, it is difficult to assign the slow phases to a specific event in the reaction progression. It may reflect a slow protein conformational change that occurs after formation of the most stable intermediate. Alternatively, it might reflect progression forward to an intermediate with nearly identical absorption maxima but a greater molar extinction coefficient.

A structure of *E. coli* SufS trapped in an external aldimine state through the use of the substrate analog L-propargylamine was interpreted to indicate that no conformational changes occur during the cysteine desulfurase reaction cycle (22). The lack of conformational change in the SufS-L-propargylamine structure is explained by the fact that the analog possesses a $C_\gamma$ atom rather than the $S_\gamma$ of Cys so that the hydrogen bonding interactions to Arg-56 or Arg-359 cannot occur. Additionally, the analog C$\gamma$ atom was disordered and not visible in electron density and therefore the structure more appropriately models a product complex than a substrate complex (22). We identified both local and long-range conformational changes associated with cysteine desulfurase reaction intermediates. Arg-56 and Arg-359 undergo changes to assist in positioning Cys-aldimine for $C_\alpha$–H bond cleavage. Cys-364 hydrogen bonding to Cys is also required for correct positioning of Cys-aldimine. The structure reported herein is the first observation of a cysteine desulfurase captured with a Cys-aldimine intermediate. The structure is consistent with the principles of PLP facilitated chemistry: only a small rotation is required to place $C_\alpha$–H perpendicular to the pyridine ring of PLP, the ideal location for promoting $C_\alpha$–H bond breaking (39, 40). The dynamics of the $\alpha$3–$\alpha$4 loop of SufS, which contains Arg-56, have also been identified as important during SufS binding to SufE/SufU, indicating there are multiple functional roles for this active-site "flap" (41, 42). The global rotation of the SufS monomers relative to each other in the Cys-ketimine state can be compared with previous studies showing that formation of an active-site persulfide alters SufS dynamics (25). HDX-MS and structural data of SufS dimer interface mutants identified a pathway for active-site cross-talk in the SufS homodimer (23). The conformational changes observed in Fig. 7*D* are reminiscent of the monomer rotations associated with transpersulfuration and indicate that the monomers rearrange relative to each other during both the desulfurase and transpersulfuration reactions. Mounting evidence infers both local and global conformational changes are required for SufS function.

We examined how widely these functional roles may be conserved in SufS family enzymes, by constructing a multiple sequence alignment of members spanning the sequence diversity of IPR010970 and found that Arg-56, His-123, and Cys-364 are conserved in all sequences inspected (Fig. 1). Additionally,

structural superpositions of SufS family members with known structures indicated these active-site amino acids occupy similar positions in all known structures (Fig. 1). For these reasons we believe sulfur mobilization by SufS occurs by a conserved mechanism in all family members.

Two main structural differences in the vicinity of the active-site distinguish type I from type II cysteine desulfurases: the presence of the extended flexible loop containing the active-site Cys in type I enzymes and the presence of the β-hairpin (or β-hook) in type II enzymes (18, 42). These structural differences provide the possibility for diverging dynamics and mechanisms in the two types of cysteine desulfurases. However, structural superpositions of the type I *E. coli* IscS with SufS illustrate that Arg-56 and His-123 are conserved and occupy a similar structural environment (data not shown). Mammalian selenocysteine lyases are also PLP-dependent enzymes with structural similarity to SufS and recent studies indicate that an active-site Cys is required for positioning selenocysteine to promote external aldimine formation (43). Additionally, it was observed that mammalian selenocysteine lyase undergoes an "open to closed" rotation of the dimer subunits reminiscent of the rotation of SufS in the Cys-ketimine state (Fig. 7) (43). We believe our identification of the functional role of SufS active-site residues and the accompanying structural model for reaction progression will provide a testable model for analysis of diverse cysteine desulfurases and related enzymes.

## Experimental procedures

### *Strains and plasmid preparation*

SufS, SufS mutants, and SufE were all expressed using the pET21a vector (Novagen) as previously described (9). SufS H123A and SufS C364A mutations were constructed following the QuikChange II site-directed mutagenesis protocol (Agilent) with mutations confirmed via sequencing. Each plasmid was transformed into BL21(DE3) *E. coli* cells for expression and purification. All primers and strains are defined in Tables S1 and S2 respectively.

### *Protein expression and purification*

SufS, SufS mutant derivatives, and SufE were expressed in the pET21a vector using BL21(DE3) *E. coli* cells. Cells grown overnight in LB with 100 μg/ml of ampicillin at 37 °C were diluted by 1:100 into fresh LB with ampicillin and incubated with shaking at 200 rpm to reach an $A_{600}$ of 0.5–0.7.

For SufS expression, cells were induced with 500 μM isopropyl β-D-1-thiogalactopyranoside at 18 °C for 24 h with shaking at 200 rpm. Cells were harvested via centrifugation at 7,460 × *g* for 10 min at 4 °C and stored at −80 °C until use. These cells were then resuspended in the Q-Sepharose loading buffer consisting of 25 mM Tris-HCl, pH 8.0, 10 mM β-mercaptoethanol (βME), and 1 mM phenylmethylsulfonyl fluoride. For lysis, two 2-min cycles of sonication at 50% amplitude of 1-s on and 2 s off were performed using a Branson digital sonifier 450. 1% Streptomycin sulfate was then added to the lysed cells followed by centrifugation at 31,000 × *g* for 35 min. SufS and SufS mutants were purified with anion exchange (Q-Sepharose), hydrophobic interaction (Phenyl FF), and gel filtration (Superdex 200) (GE Healthcare) chromatography resins in sequence. The Q-Sepharose column used a linear gradient from 25 mM Tris-HCl, pH 8.0, 10 mM βME to 25 mM Tris-HCl, pH 8.0, 1 M NaCl, 10 mM βME. For the phenyl FF column, SufS was eluted using a linear gradient from 25 mM Tris-HCl, pH 8.0, 100 mM NaCl, 1 M ammonium sulfate, 10 mM βME to 25 mM Tris-HCl, pH 8.0, 10 mM βME. The Superdex 200 column was run with 25 mM Tris-HCl, pH 8.0, 150 mM NaCl, 10 mM βME. Final protein purity was evaluated using SDS-PAGE and the protein was concentrated via a 10-kDa molecular mass Amicon Ultra concentration filter (Millipore). Purified SufS was frozen in liquid nitrogen and stored at −80 °C until further use. Further detail of this purification can be found in the supporting information.

SufE expression was performed using a similar protocol as SufS with a few modifications. For SufE, cells were induced with 500 μM isopropyl β-D-1-thiogalactopyranoside at 37 °C for 3 h with shaking at 200 rpm. SufE purification used anion exchange and gel filtration chromatography for purification. The buffers were the same as those used for SufS purification.

### *PLP quantification*

To determine PLP content of SufS, SufS was diluted to ~1.5 mg/ml as part of an 800-μl sample using 10 mM Tris, pH 8.0, buffer. 200 μl of 5 M NaOH was added to the protein and incubated for 10 min at 75 °C. 85 μl of 12 M HCl was then added to the sample. Denatured SufS protein was removed by centrifugation at 16,000 × *g* for 2 min. The supernatant containing released PLP was transferred to a cuvette. The absorbance at 390 nm was measured with the resulting value compared with a free PLP quantification standard line to determine the amount of PLP present. PLP occupancy per monomer of SufS was then calculated based on molar ratios of PLP:SufS monomer.

### *Cysteine desulfurase activity assay*

SufS cysteine desulfurase activity was determined by following the protocol used by Dai and Outten (9). For reactions involving SufS and SufE, concentrations of 0.5 and 2.0 μM were used, respectively. With SufS or SufS mutants alone, the selected concentration was either 0.5 or 20 μM. The reaction was performed at room temperature for 10 min.

### *UV-visible absorption spectroscopy*

Using an Agilent 8453 UV-visible absorption spectrophotometer, both spectra and kinetics were monitored for extended time periods. 30 μM WT, H123A, or C364A SufS was treated with 500 μM cysteine in the presence of 2 mM tris(2-carboxyethyl)phosphine in buffer (25 mM Tris, 150 mM NaCl, pH 7.4). Initial scans were measured 10 s after mixing with final scans occurring at 150 min.

### *Stopped-flow absorption spectroscopic analysis*

Stopped-flow absorption experiments were performed at 4 °C on an Applied Photophysics Ltd. SX20 stopped-flow spectrophotometer equipped with an anaerobic accessory using either a PDA or PMT. L-Cysteine was prepared anaerobically in anoxic 25 mM Tris, 150 mM NaCl at pH 8.0 (at 4 °C) within a crimped vial to remain anaerobic. WT-SufS (or variant) was diluted at 4 °C to 75 μM using 25 mM Tris, 150 mM NaCl, pH 8.0. Concentrations of cysteine ranging from 800 μM to 3 mM (pre-

**Table 3**
**Data collection and refinement statistics**

| | WT Cys soak 6O10 | C364A Cys-ald 6O11 | | H123A 6O12 | H123A Cys-ket 6O13 | |
|---|---|---|---|---|---|---|
| | Native | Native | Anomalous | Native | Native | Anomalous |
| **Data collection** | APS 22-ID | APS 22-ID | APS 22-ID | APS 22-ID | APS 22-ID | APS 22-ID |
| Space group | $P4_32_12$ | $P4_22_12$ | $P4_22_12$ | $P4_32_12$ | $P4_32_12$ | $P4_32_12$ |
| Cell dimensions | | | | | | |
| *a*, *b*, *c* (Å) | 126.40, 126.40, 133.68 | 126.42, 126.42, 67.08 | 126.58, 126.58, 67.12 | 127.28, 127.28,134.16 | 126.01, 126.01 137.21 | 126.02, 126.02, 137.00 |
| $\alpha, \beta, \gamma$ (°) | 90, 90, 90 | 90, 90, 90 | 90, 90, 90 | 90, 90, 90 | 90, 90, 90 | 90, 90, 90 |
| Wavelength | 1.000 | 1.000 | 1.740 | 1.000 | 1.000 | 1.740 |
| Resolution (Å) | 44.69–2.00 (2.07–2.00) | 35.69–1.84 (1.90–1.84) | 89.50–3.90 (4.00–3.90) | 43.40–2.05 (2.12–2.05) | 44.55–2.20 (2.28–2.20) | 92.75–3.20 (3.28–3.20) |
| $R_{meas}$ (%) | 11.3 (421.1) | 8.5 (200.0) | 5.1 (6.6) | 17.5 (282.2) | 11.7 (211.9) | 13.3 (41.0) |
| $I/\sigma I$ | 17.26 (0.84) | 15.51 (0.76) | 43.68 (36.39) | 15.92 (0.68) | 12.71 (1.14) | 16.33 (7.21) |
| Completeness (%) | 99.9 (99.8) | 97.9 (83.8) | 99.9 (100.0) | 99.2 (95.0) | 99.9 (99.5) | 100.0 (100.0) |
| Redundancy | 26.7 (24.9) | 11.8 (6.7) | 12.2 (12.6) | 6.7 (6.0) | 14.8 (15.0) | 13.8 (15.4) |
| $CC_{1/2}$ (%) | 99.9 (36.7) | 99.9 (49.6) | 99.9 (99.9) | 99.1(45.7) | 99.8(61.0) | 99.7 (97.7) |
| **Refinement** | | | | | | |
| Resolution (Å) | 44.69–2.00 (2.07–2.00) | 35.69–1.84 (1.90–1.84) | | 43.40–2.05 (2.12–2.05) | 44.55–2.20 (2.28 - 2.20) | |
| No. reflections | 73,439 (7,236) | 46,697 (3,927) | | 68,944 (6,521) | 56,320 (5,508) | |
| $R_{work}/R_{free}$ (%) | 18.24(31.42)/ 20.39(35.81) | 18.38 (34.21)/ 21.62 (36.07) | | 19.45 (35.09)/ 21.59 (37.08) | 18.73 (35.23)/19.86 (36.14) | |
| No. atoms | 3,308 | 3,245 | | 3216 | 3,234 | |
| Protein | 3,119 | 3,126 | | 3114 | 3,122 | |
| Ligand | 16 | 23 | | 16 | 23 | |
| Water | 173 | 96 | | 86 | 89 | |
| *B* factors | | | | | | |
| Protein | 53.66 | 48.81 | | 39.56 | 65.59 | |
| Ligand | 45.88 | 40.21 | | 42.20 | 62.66 | |
| Water | 58.38 | 49.43 | | 39.52 | 67.26 | |
| Root mean square deviations | | | | | | |
| Bond lengths (Å) | 0.007 | 0.006 | | 0.008 | 0.007 | |
| Bond angles (°) | 0.92 | 0.81 | | 0.85 | 0.92 | |

mix) were mixed 1:1 with 75 $\mu$M SufS for a post-mix SufS concentration of 37.5 $\mu$M. Full spectral (PDA) or single wavelength (PMT) data were collected out at 5 to 20 s, depending on cysteine concentration. Data were then fit to a double exponential model using Pro Data Viewer version 4.2.18 (APP) (Figs. S5–S7).

### *Global analysis and singular value decomposition*

PDA data were analyzed using SVD with Pro-KIV global analysis software (APP). SVD fitting for H123A showed two non-zero singular values corresponding to two transitions between three spectrally distinct species. To process the data, the following model was used in which $k_1'$ characterizes a pseudo first-order rate constant during which L-cysteine concentrations are in large excess compared with the enzyme.

$$\text{SufS-PLP} + \text{L-Cys} \xrightarrow{k_1'} \text{Int-1} \xrightarrow{k_2} \text{Int-2} \qquad \text{(Eq. 1)}$$

For the above model, initial rates for input were determined via single-wavelength kinetics using the PMT. The final rate constants calculated by global analysis demonstrated favorable agreement with these PMT values.

### *X-ray crystallography*

Crystallization of SufS WT was performed by mixing 1 $\mu$l of protein at ~10 mg/ml with 2 $\mu$l of 4.3 M NaCl and 0.1 M MES, pH 6.5, followed by incubation at 20 °C in sitting drop vapor diffusion trays (24). Crystallization of SufS H123A was performed by mixing 1 $\mu$l of protein at 12 mg/ml with 2 $\mu$l of 4.3 M NaCl and 0.1 M MES, pH 6.5 (PLP bound structure), or 2 $\mu$l of 4.0 M NaCl and 0.1 M MES, pH 6.5 (Cys-ketimine structure). In both cases incubation at 20 °C in sitting drop vapor diffusion trays occurred. Crystals typically formed in less than 7 days. To obtain the structure of SufS H123A in the absence of substrate, H123A crystals were incubated in mother liquor diluted 1:1 with 100% (v/v) glycerol followed by plunge freezing in liquid $N_2$. To obtain the structures of SufS WT and SufS His-123 following L-cysteine addition, crystals were incubated in mother liquor plus 10 mM L-cysteine diluted 1:1 with 100% (v/v) glycerol. The crystals were plunge frozen in liquid $N_2$ following 5–30 min incubation with L-cysteine.

Crystallization of SufS C364A was performed by mixing 1 $\mu$l of 14 mg/ml of protein with 2 $\mu$l of crystallization conditions (20–30% (w/v) PEG 3350, 0.1 M Tris-HCl, pH 7, 0.2 M $MgCl_2$) followed by incubation at 20 °C in sitting drop vapor diffusion trays. Addition of L-cysteine to SufS C364A was accomplished by incubating the crystals in mother liquor plus 50 mM L-cysteine diluted 1:1 with 100% (v/v) glycerol. The crystals were incubated at −20 °C for 30 min, warmed to 37 °C for 30 min, then allowed to return to room temperature before plunge freezing in liquid $N_2$. Structures were solved using crystals with and without the temperature cycling step revealing it is not required to obtain the Cys-aldimine intermediate, but the best diffracting crystals underwent temperature cycling.

Native X-ray diffraction data were collected at the Advanced Photon Source beamline 22-ID, outfitted with an Eiger 16 M detector, using 0.5° oscillations and a 1.000-Å wavelength. Anomalous X-ray diffraction data were collected at 22-ID using 1.74-Å wavelength X-rays.

Reflections were integrated and merged using X-ray Detector Software. Structure solution was carried out by molecular replacement in the PHENIX software suite using PDB 1jf9 with all heteroatoms removed as the search model (24). Phenix.refine was used to improve the initial structure solutions and generate the unbiased $F_o - F_c$ maps indicating ligand electron density. Initial coordinates and refinement restraints for PLP linked to Cys-aldimine or Cys-ketimine were generated by phenix.elbow and the models were improved by iterative cycles of manual modeling in Coot coupled with phenix.refine. Occupancy refinement of PLP Cys-aldimine and PLP Cys-ketimine was performed once the final model was obtained and atomic displacement parameters (B-factors) refinement had converged. Anomalous maps were calculated using phenix.maps with phases derived from coordinates without ligands.

Figures were generated with PyMol. Superpositions were performed by aligning one SufS monomer to the SufS variant monomer with the PyMol align command. Data collection and refinement statistics can be found in Table 3.

### *Sequence conservation analysis*

A sequence similarity network was constructed from 18,567 sequences of the SufS Interpro family IPR010970 as previously described (23). Briefly, sequences with an alignment score of 45 or better were binned to create 1011 nodes. Of these nodes, 29 composed of >100 sequences were chosen for further analysis. One representative sequence was chosen from the 29 nodes with preference given to Swiss-Prot reviewed entries. The representative sequences were aligned with MUltiple Sequence Comparison by Log-Expectation (MUSCLE) and the resulting alignment was used to estimate the conservation of SufS residues (44).

*Author contributions*—M. B. and M. R. B. investigation; M. B., C. E. W., M. R. B., P. A. F., and J. A. D. visualization; M. B., C. E. W., G. D., and J. A. D. methodology; M. B. and G. D. writing-original draft; C. E. W., M. R. B., and T. M. M. software; C. E. W., T. M. M., and J. A. D. formal analysis; M. R. B. data curation; G. D., P. A. F., J. A. D., and F. W. O. conceptualization; T. M. M., J. A. D., and F. W. O. supervision; T. M. M., P. A. F., and J. A. D. validation; T. M. M., P. A. F., J. A. D., and F. W. O. writing-review and editing; P. A. F. and F. W. O. funding acquisition; J. A. D. project administration; J. A. D. co-corresponding author.

*Acknowledgments—We thank Dr. Job Grant for initial assistance with early SVD analysis. Data were collected at Southeast Regional Collaborative Access Team (SER-CAT) 22-ID (or 22-BM) beamline at the Advanced Photon Source, Argonne National Laboratory. SER-CAT is supported by its member institutions (https://www.ser.aps.anl.gov/),[4] and equipment grants (S10_RR25528 and S10_RR028976) from the National Institutes of Health. Use of the Advanced Photon Source was supported by the U. S. Department of Energy, Office of Science, Office of Basic Energy Sciences, under Contract no. W-31-109-Eng-38.*

[4] Please note that the JBC is not responsible for the long-term archiving and maintenance of this site or any other third party hosted site.

## References


1. Fontecave, M. (2006) Iron-sulfur clusters: ever-expanding roles. *Nat. Chem. Biol.* **2,** 171–174 CrossRef Medline
2. Volbeda, A., Charon, M. H., Piras, C., Hatchikian, E. C., Frey, M., and Fontecilla-Camps, J. C. (1995) Crystal structure of the nickel-iron hydrogenase from *Desulfovibrio gigas*. *Nature* **373,** 580–587 CrossRef Medline
3. Roche, B., Aussel, L., Ezraty, B., Mandin, P., Py, B., and Barras, F. (2013) Iron/sulfur proteins biogenesis in prokaryotes: formation, regulation and diversity. *Biochim. Biophys. Acta* **1827,** 455–469 CrossRef Medline
4. Tokumoto, U., and Takahashi, Y. (2001) Genetic analysis of the *isc* operon in *Escherichia coli* involved in the biogenesis of cellular iron-sulfur proteins. *J. Biochem.* **130,** 63–71 CrossRef Medline
5. Fontecave, M., Choudens, S. O., Py, B., and Barras, F. (2005) Mechanisms of iron-sulfur cluster assembly: the SUF machinery. *J. Biol. Inorg. Chem.* **10,** 713–721 CrossRef Medline
6. Nachin, L., Loiseau, L., Expert, D., and Barras, F. (2003) SufC: an unorthodox cytoplasmic ABC/ATPase required for [Fe-S] biogenesis under oxidative stress. *EMBO J.* **22,** 427–437 CrossRef Medline
7. Outten, F. W., Djaman, O., and Storz, G. (2004) A suf operon requirement for Fe-S cluster assembly during iron starvation in *Escherichia coli*. *Mol. Microbiol.* **52,** 861–872 CrossRef Medline
8. Mihara, H., Maeda, M., Fujii, T., Kurihara, T., Hata, Y., and Esaki, N. (1999) A nifS-like gene, *csdB*, encodes an *Escherichia coli* counterpart of mammalian selenocysteine lyase: gene cloning, purification, characterization and preliminary x-ray crystallographic studies. *J. Biol. Chem.* **274,** 14768–14772 CrossRef Medline
9. Dai, Y., and Outten, F. W. (2012) The *E. coli* SufS-SufE sulfur transfer system is more resistant to oxidative stress than IscS-IscU. *FEBS Lett.* **586,** 4016–4022 CrossRef Medline
10. Selbach, B. P., Pradhan, P. K., and Dos Santos, P. C. (2013) Protected sulfur transfer reactions by the *Escherichia coli* Suf system. *Biochemistry* **52,** 4089–4096 CrossRef Medline
11. Mihara, H., Kurihara, T., Yoshimura, T., Soda, K., and Esaki, N. (1997) Cysteine sulfinate desulfinase, a NIFS-like protein of *Escherichia coli* with selenocysteine lyase and cysteine desulfurase activities: gene cloning, purification, and characterization of a novel pyridoxal enzyme. *J. Biol. Chem.* **272,** 22417–22424 CrossRef Medline
12. Fujii, T., Maeda, M., Mihara, H., Kurihara, T., Esaki, N., and Hata, Y. (2000) Structure of a NifS homologue: X-ray structure analysis of CsdB, an *Escherichia coli* counterpart of mammalian selenocysteine lyase. *Biochemistry* **39,** 1263–1273 CrossRef Medline
13. Tirupati, B., Vey, J. L., Drennan, C. L., and Bollinger, J. M., Jr. (2004) Kinetic and structural characterization of Slr0077/SufS, the essential cysteine desulfurase from *Synechocystis* sp. PCC 6803. *Biochemistry* **43,** 12210–12219 CrossRef Medline
14. Trotter, V., Vinella, D., Loiseau, L., Ollagnier de Choudens, S., Fontecave, M., and Barras, F. (2009) The CsdA cysteine desulphurase promotes Fe/S biogenesis by recruiting Suf components and participates to a new sulphur transfer pathway by recruiting CsdL (ex-YgdL), a ubiquitin-modifying-like protein. *Mol. Microbiol.* **74,** 1527–1542 CrossRef Medline
15. Loiseau, L., Ollagnier-de-Choudens, S., Nachin, L., Fontecave, M., and Barras, F. (2003) Biogenesis of Fe-S cluster by the bacterial Suf system: SufS and SufE form a new type of cysteine desulfurase. *J. Biol. Chem.* **278,** 38352–38359 CrossRef Medline
16. Outten, F. W., Wood, M. J., Munoz, F. M., and Storz, G. (2003) The SufE protein and the SufBCD complex enhance SufS cysteine desulfurase activity as part of a sulfur transfer pathway for Fe-S cluster assembly in *Escherichia coli*. *J. Biol. Chem.* **278,** 45713–45719 CrossRef Medline
17. Layer, G., Gaddam, S. A., Ayala-Castro, C. N., Ollagnier-de Choudens, S., Lascoux, D., Fontecave, M., and Outten, F. W. (2007) SufE transfers sulfur from SufS to SufB for iron-sulfur cluster assembly. *J. Biol. Chem.* **282,** 13342–13350 CrossRef Medline
18. Black, K. A., and Dos Santos, P. C. (2015) Shared-intermediates in the biosynthesis of thio-cofactors: mechanism and functions of cysteine desulfurases and sulfur acceptors. *Biochim. Biophys. Acta* **1853,** 1470–1480 CrossRef Medline
19. Zheng, L., White, R. H., Cash, V. L., and Dean, D. R. (1994) Mechanism for the desulfurization of L-cysteine catalyzed by the *nifS* gene product. *Biochemistry* **33,** 4714–4720 CrossRef Medline
20. Behshad, E., and Bollinger, J. M., Jr. (2009) Kinetic analysis of cysteine desulfurase CD0387 from *Synechocystis* sp. PCC 6803: formation of the persulfide intermediate. *Biochemistry* **48,** 12014–12023 CrossRef Medline
21. Mihara, H., Kurihara, T., Yoshimura, T., and Esaki, N. (2000) Kinetic and mutational studies of three NifS homologs from *Escherichia coli*: mechanistic difference between L-cysteine desulfurase and L-selenocysteine lyase reactions. *J. Biochem.* **127,** 559–567 CrossRef Medline
22. Mihara, H., Fujii, T., Kato, S., Kurihara, T., Hata, Y., and Esaki, N. (2002) Structure of external aldimine of *Escherichia coli* CsdB, an IscS/NifS homolog: implications for its specificity toward selenocysteine. *J. Biochem.* **131,** 679–685 CrossRef Medline
23. Dunkle, J. A., Bruno, M. R., Outten, F. W., and Frantom, P. A. (2019) Structural evidence for dimer-interface-driven regulation of the type II cysteine desulfurase, SufS. *Biochemistry* **58,** 687–696 CrossRef Medline
24. Lima, C. D. (2002) Analysis of the *E. coli* NifS CsdB protein at 2.0 Å reveals the structural basis for perselenide and persulfide intermediate formation. *J. Mol. Biol.* **315,** 1199–1208 CrossRef Medline
25. Kim, D., Singh, H., Dai, Y., Dong, G., Busenlehner, L. S., Outten, F. W., and Frantom, P. A. (2018) Changes in protein dynamics in *Escherichia coli* SufS reveal a possible conserved regulatory mechanism in type II cysteine desulfurase systems. *Biochemistry* **57,** 5210–5217 CrossRef Medline
26. Van Hoewyk, D., Abdel-Ghany, S. E., Cohu, C. M., Herbert, S. K., Kugrens, P., Pilon, M., and Pilon-Smits, E. A. (2007) Chloroplast iron-sulfur cluster protein maturation requires the essential cysteine desulfurase CpNifS. *Proc. Natl. Acad. Sci. U.S.A.* **104,** 5686–5691 CrossRef Medline
27. Albrecht, A. G., Peuckert, F., Landmann, H., Miethke, M., Seubert, A., and Marahiel, M. A. (2011) Mechanistic characterization of sulfur transfer from cysteine desulfurase SufS to the iron-sulfur scaffold SufU in *Bacillus subtilis*. *FEBS Lett.* **585,** 465–470 CrossRef
28. Zhou, X., and Toney, M. D. (1999) pH studies on the mechanism of the pyridoxal phosphate-dependent dialkylglycine decarboxylase. *Biochemistry* **38,** 311–320 CrossRef Medline
29. Karsten, W. E., and Cook, P. F. (2009) Detection of a gem-diamine and a stable quinonoid intermediate in the reaction catalyzed by serine-glyoxylate aminotransferase from *Hyphomicrobium methylovorum*. *Biochim. Biophys. Acta* **1790,** 575–580 CrossRef
30. Phillips, R. S. (2011) Structure, mechanism, and substrate specificity of kynureninase. *Biochim. Biophys. Acta* **1814,** 1481–1488 CrossRef Medline
31. Sun, S., and Toney, M. D. (1999) Evidence for a two-base mechanism involving tyrosine-265 from arginine-219 mutants of alanine racemase. *Biochemistry* **38,** 4058–4065 CrossRef Medline
32. Hirayama, A., Miyanaga, A., Kudo, F., and Eguchi, T. (2015) Mechanism-based trapping of the quinonoid intermediate by using the K276R mutant of PLP-dependent 3-aminobenzoate synthase PctV in the biosynthesis of pactamycin. *Chembiochem* **16,** 2484–2490 CrossRef Medline
33. Kaiser, J. T., Bruno, S., Clausen, T., Huber, R., Schiaretti, F., Mozzarelli, A., and Kessler, D. (2003) Snapshots of the cystine lyase C-DES during catalysis: studies in solution and in the crystalline state. *J. Biol. Chem.* **278,** 357–365 CrossRef Medline
34. Campanini, B., Schiaretti, F., Abbruzzetti, S., Kessler, D., and Mozzarelli, A. (2006) Sulfur mobilization in cyanobacteria: the catalytic mechanism of L-cystine C-S lyase (C-DES) from *synechocystis*. *J. Biol. Chem.* **281,** 38769–38780 CrossRef
35. Soniya, K., and Chandra, A. (2018) Free energy landscapes of prototropic tautomerism in pyridoxal 5′-phosphate schiff bases at the active site of an enzyme in aqueous medium. *J. Comput. Chem.* **39,** 1629–1638 CrossRef Medline
36. Liang, J., Han, Q., Tan, Y., Ding, H., and Li, J. (2019) Current advances on structure-function relationships of pyridoxal 5′-phosphate-dependent enzymes. *Front. Mol. Biosci.* **6,** 4 CrossRef Medline
37. Singh, H., Dai, Y., Outten, F. W., and Busenlehner, L. S. (2013) *Escherichia coli* SufE sulfur transfer protein modulates the SufS cysteine desulfurase through allosteric conformational dynamics. *J. Biol. Chem.* **288,** 36189–36200 CrossRef Medline

38. Dai, Y., Kim, D., Dong, G., Busenlehner, L. S., Frantom, P. A., and Outten, F. W. (2015) SufE D74R substitution alters active site loop dynamics to further enhance SufE interaction with the SufS cysteine desulfurase. *Biochemistry* **54,** 4824–4833 CrossRef Medline
39. Eliot, A. C., and Kirsch, J. F. (2004) Pyridoxal phosphate enzymes: mechanistic, structural, and evolutionary considerations. *Annu. Rev. Biochem.* **73,** 383–415 CrossRef Medline
40. Toney, M. D. (2011) Controlling reaction specificity in pyridoxal phosphate enzymes. *Biochim. Biophys. Acta* **1814,** 1407–1418 CrossRef Medline
41. Kim, S., and Park, S. (2013) Structural changes during cysteine desulfurase CsdA and sulfur acceptor CsdE interactions provide insight into the transpersulfuration. *J. Biol. Chem.* **288,** 27172–27180 CrossRef Medline
42. Blauenburg, B., Mielcarek, A., Altegoer, F., Fage, C. D., Linne, U., Bange, G., and Marahiel, M. A. (2016) Crystal structure of *Bacillus subtilis* cysteine desulfurase SufS and its dynamic interaction with Frataxin and scaffold protein SufU. *PLoS ONE* **11,** e0158749 CrossRef Medline
43. Omi, R., Kurokawa, S., Mihara, H., Hayashi, H., Goto, M., Miyahara, I., Kurihara, T., Hirotsu, K., and Esaki, N. (2010) Reaction mechanism and molecular basis for selenium/sulfur discrimination of selenocysteine lyase. *J. Biol. Chem.* **285,** 12133–12139 CrossRef Medline
44. Edgar, R. C. (2004) MUSCLE: multiple sequence alignment with high accuracy and high throughput. *Nucleic Acids Res.* **32,** 1792–1797 CrossRef Medline

# Direct observation of intermediates in the SufS cysteine desulfurase reaction reveals functional roles of conserved active-site residues

Matthew Blahut, Courtney E. Wise, Michael R. Bruno, Guangchao Dong, Thomas M. Makris, Patrick A. Frantom, Jack A. Dunkle and F. Wayne Outten

*J. Biol. Chem. 2019, 294:12444-12458.*
*doi: 10.1074/jbc.RA119.009471 originally published online June 27, 2019*